Cell Reports
Report

Essential Regulation of Lung Surfactant Homeostasis by the Orphan G Protein-Coupled Receptor GPR116

Mi Young Yang,[1] Mary Beth Hilton,[1,2] Steven Seaman,[1] Diana C. Haines,[5] Kunio Nagashima,[4] Christina M. Burks,[5] Lino Tessarollo,[3] Pavlina T. Ivanova,[6] H. Alex Brown,[6] Todd M. Umstead,[7] Joanna Floros,[7,8] Zissis C. Chroneos,[7] and Brad St. Croix[1,*]

[1]Tumor Angiogenesis Section, Mouse Cancer Genetics Program (MCGP), Center for Cancer Research (CCR)
[2]SAIC-Frederick, Frederick National Laboratory for Cancer Research (FNLCR)
[3]Neural Development Section, MCGP, CCR
[4]Electron Microscopy Laboratory, Advanced Technology Program, SAIC-Frederick, FNLCR
[5]Veterinary Pathology Section, Pathology/Histotechnology Laboratory, SAIC-Frederick, FNLCR
National Cancer Institute (NCI), Frederick, MD 21702, USA
[6]Department of Pharmacology and the Vanderbilt Institute of Chemical Biology, Vanderbilt University Medical Center, Nashville, TN 37232, USA
[7]Department of Pediatrics and Center for Host defense, Inflammation, and Lung Disease Research
[8]Department of Obstetrics and Gynecology
The Pennsylvania State University College of Medicine, 500 University Drive, Hershey, PA 17033, USA
*Correspondence: stcroix@ncifcrf.gov
http://dx.doi.org/10.1016/j.celrep.2013.04.019

SUMMARY

GPR116 is an orphan seven-pass transmembrane receptor whose function has been unclear. Global disruption of the *Gpr116* gene in mice revealed an unexpected, critical role for this receptor in lung surfactant homeostasis, resulting in progressive accumulation of surfactant lipids and proteins in the alveolar space, labored breathing, and a reduced lifespan. GPR116 expression analysis, bone marrow transplantation studies, and characterization of conditional knockout mice revealed that GPR116 expression in ATII cells is required for maintaining normal surfactant levels. Aberrant packaging of surfactant proteins with lipids in the *Gpr116* mutant mice resulted in compromised surfactant structure, function, uptake, and processing. Thus, GPR116 plays an indispensable role in lung surfactant homeostasis with important ramifications for the understanding and treatment of lung surfactant disorders.

INTRODUCTION

The vital process of mammalian breathing requires alveoli to expand and contract without collapsing, a remarkable feat that depends upon the surface tension-reducing properties of the lipid-rich surfactant film that lines the alveolus (Trapnell et al., 2003). Pulmonary surfactant, which also functions in innate immunity, is composed of 90% lipids (primarily phosphatidylcholine [PC]) and 10% protein (surfactant proteins A [SP-A], SP-B, SP-C, and SP-D). In premature infants, insufficient production of surfactant leads to neonatal respiratory distress syndrome (RDS). Surfactant deficiency also contributes to the pathogenesis of acute lung injury (ALI) and acute RDS (ARDS), disorders that can afflict patients of all ages and carry a mortality rate greater than 25% (Lewis and Veldhuizen, 2006; Raghavendran et al., 2011). Conversely, accumulation of surfactant in the alveolar space leads to pulmonary alveolar proteinosis (PAP) (Carey and Trapnell, 2010). Although important progress has been made in understanding surfactant catabolism by macrophages, a process dependent upon GM-CSF signaling (Carey and Trapnell, 2010; Sakagami et al., 2009), mechanisms regulating surfactant homeostasis in the alveolar space remain largely unexplained. Furthermore, whole-lung lavage, the standard of care for PAP, only helps a subset of patients, has numerous complications, and does not address the pathogenic mechanisms at work (Borie et al., 2011). Thus, new methods of regulating surfactant levels and activity are urgently needed and could have an impact on a myriad of lung diseases.

RESULTS AND DISCUSSION

Genetic Disruption of *Gpr116* Results in a Shortened Lifespan Associated with Pulmonary-Specific Abnormalities

G protein-coupled receptor (GPCR) superfamily members mediate cell signaling in response to a diverse array of extracellular stimuli and comprise over one-third of the drug targets of modern medicine (Tang et al., 2012). While searching a large panel of gene expression libraries for endothelial GPCRs (Seaman et al., 2007; St Croix et al., 2000), we identified *Gpr116*, also called Ig-Hepta in rats (Abe et al., 1999), as a pan-endothelial-expressed gene of unknown function (Figures S1A–S1H; see also Wallgard et al., 2008). *Gpr116* was broadly expressed in normal unfractionated tissues with highest expression in lung

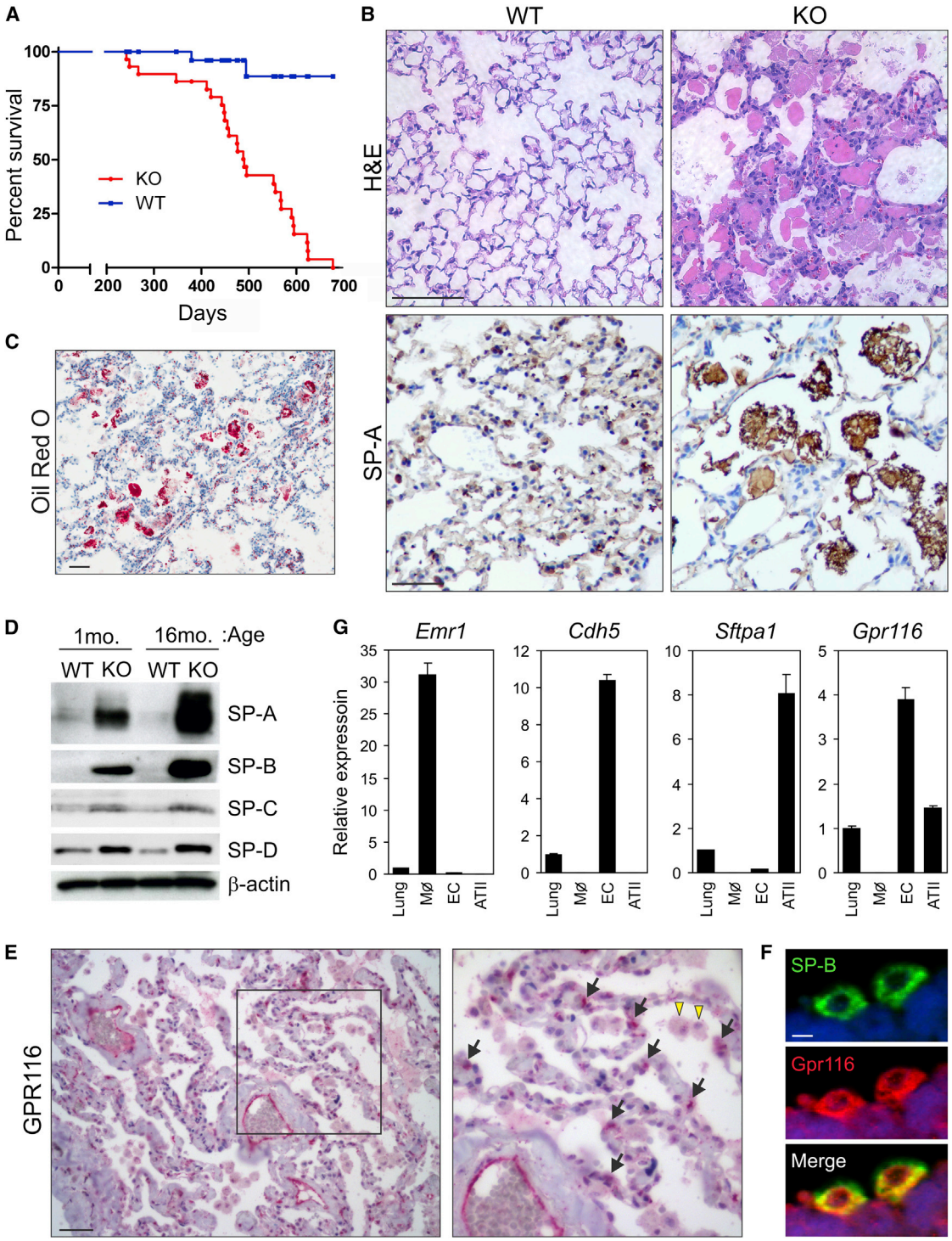

Figure 1. *Gpr116* Is Expressed in Lung ECs and ATII Cells and Is Important for Maintaining Lung Surfactant Homeostasis

(A) Survival analysis of *Gpr116* WT and KO mice.

(B) An accumulation of eosinophilic, SP-A+ material was observed in the alveolar space of 6-month-old lungs of KO mice by H&E and SP-A staining. Scale bar, 50 μm.

(C) The accumulated lung material stained positive with oil red O dye indicative of a buildup of neutral lipids in the alveolar space. Scale bar, 50 μm.

(D) Immunoblotting for SP-A, SP-B, SP-C, and SP-D in KO versus WT whole-lung lysates.

(E) Immunohistochemical staining of normal human lung. GPR116 protein (red) can be found in both ECs and ATII cells (arrows in inset), whereas alveolar macrophages were negative (yellow arrowheads). Scale bar, 100 μm.

(legend continued on next page)

(Abe et al., 1999) (Figure S1C). To explore the function of GPR116, we generated *Gpr116*$^{-/-}$ knockout (KO) mice by removing exon 2 containing the start codon and signal peptide (Figures S1I–S1L). *Gpr116* KO mice were viable and fertile but displayed labored breathing by 4 months of age, weighed up to 25% less than wild-type (WT) littermates by 14 months, and had a shortened lifespan (Figures 1A and S2A). A complete histopathological survey of 6-month-old mice revealed defects only in the KO lung, whereas heterozygous mice were normal. A PAP-like phenotype was observed in the KO, which included a striking accumulation of eosinophilic, periodic acid-Schiff (PAS)-positive material in the alveolar space (Figures 1B and S2B). Oil red O staining confirmed the buildup of lipids in the alveolar material that also stained positive for SP-A by immunohistochemistry (Figures 1B and 1C). Immunoblotting showed a large increase in SP-A and SP-B and a smaller increase in SP-C and SP-D in *Gpr116* KO lung samples (Figure 1D). Supraphysiologic accumulation of alveolar SP-A was apparent by 2 weeks of age and increased with time (Figures 1D and S2C).

To better understand GPR116 protein expression patterns, we performed immunohistochemical staining of human lung tissues. GPR116 was strongly expressed in lung endothelial cells (ECs) that lined blood-filled vessels (Figure 1E), consistent with the earlier mRNA expression analysis (Figure S1C). GPR116 protein was also detected in sporadic epithelial cells lining the alveoli (Figure 1E, arrows) that were subsequently identified as ATII cells based on SP-B coimmunofluorescence staining (Figure 1F). Clara cells did not stain (Figure S2D). QPCR analysis confirmed *Gpr116* expression in both ATII cells and ECs isolated from murine lung (Figure 1G).

Bronchoalveolar lavage fluid (BALF) had a milky appearance in the *Gpr116* KO (Figure 2A), similar to that observed in patients with PAP (Trapnell et al., 2003). An analysis of the BALF lipid content at 3 months revealed an 8-fold increase in PC (Figure 2B) and a 13-fold increase in cholesterol, the most abundant neutral lipid in surfactant, even though blood cholesterol levels were not significantly altered (Figure S2E). H&E of BALF cytospins revealed numerous enlarged foamy macrophages that were occasionally multinucleated (Figure 2C). By ultrastructural microscopy, alveolar spaces of the KO lungs showed an excessive number of multilamellated structures that resembled the intracytoplasmic inclusions, or lamellar bodies (LBs) of ATII cells (Figure 2D). Furthermore, macrophages were loaded with surfactant-laden phagosomes and frequently contained cholesterol clefts (Figure 2E). Thus, *Gpr116* KO mice display many of the phenotypic hallmarks of human PAP.

Lung Defects in Global *Gpr116* KO Mice Are Not Caused by Loss of GPR116 in ECs or Macrophages

The normal alveolus is lined by ATI and ATII epithelial cells that are separated from ECs by a basement membrane. To determine if GPR116+ ECs influence surfactant levels indirectly, perhaps through paracrine regulation of neighboring ATII cells or macrophages, we generated *Gpr116* conditional KO mice (*Gpr116*$^{-/flox}$, *Tie2-Cre*) that contain a *Gpr116* "floxed" allele and *Cre* driven by the *Tie2* promoter that results in deletion in ECs and a fraction of hematopoietic cells. No defects were observed despite efficient deletion of *Gpr116* in lung ECs (Figures S3A–S3D). These results suggest that a non-EC type may be responsible for driving the global *Gpr116* KO phenotype.

Autoimmune PAP is caused primarily by defects in GM-CSF signaling that result in defective catabolism of surfactant by alveolar macrophages (Borie et al., 2011; Carey and Trapnell, 2010). To determine if GM-CSF signaling in macrophages was perturbed in the *Gpr116* KO, we used QPCR to evaluate *Csf2* (*GM-CSF*) levels and critical downstream components required for macrophage differentiation and function including *Sfpi1* (PU.1), *pparg* (PPARγ), and *Abcg1* (Malur et al., 2011a; Malur et al., 2011b; Shibata et al., 2001) but did not observe any alterations in expression (Figures S3E–S3G). Furthermore, neither *Gpr116* mRNA nor GPR116 protein was detected in macrophages (Figures 1E and 1G), and *Vav-iCre* conditional *Gpr116* KO mice that deleted *Gpr116* efficiently in macrophages (Figure S3H) and possibly other vav+ leukocytes failed to develop a PAP-like phenotype (Figure S3I). We also performed bone marrow (BM) transplantation experiments and found that BM from the *Gpr116* KO was unable to transfer the PAP-like disease to WT recipients (Figure S3J). Conversely, transfer of WT *Gpr116* BM into KO mice failed to prevent the accumulation of surfactant (Figure 2F). Moreover, in the latter experiments, WT macrophages became foamy, enlarged, and binucleate, similar to that in the global KO (compare Figure 2G with Figure 2C), indicating that the KO lung microenvironment drives the abnormal macrophage phenotype. Consistent with this idea, foamy macrophages transplanted from KO lungs to surfactant-free cell culture rapidly reverted to WT size and exhibited normal phagocytic function (Figure S3K). Based on these data, we conclude that the PAP-like phenotype in the *Gpr116* KO is not driven by an autonomous macrophage defect but, rather, a distinct mechanism involving other alveolar cell type(s).

Autonomous Expression of GPR116 in ATII Cells Is Required for Normal Lung Surfactant Homeostasis

ATII cells produce surfactant and, along with macrophages, participate in its catabolism (Trapnell et al., 2003). No ultrastructural abnormalities were observed in ATII cells at 1 month. However, by 1 year, KO ATII cells displayed mild hyperplasia, increased LB size, and evidence of LB fusion (Figure S4). To determine if ATII cells were driving the global KO phenotype, we generated conditional *Gpr116* KO mice containing a floxed *Gpr116* allele and a *Cre* transgene driven by the constitutive *SFTPC* promoter. Interestingly, *SFTPC-Cre Gpr116* conditional KO mice showed a phenotype indistinguishable from the global null, including amorphous eosinophilic SP-A+ material in the alveoli (Figure 3A).

(F) Immunofluorescence staining of normal human lung. GPR116 protein (red) colocalizes with SP-B (green). Scale bar, 5 μm.
(G) QPCR analysis was used to assess *Gpr116* expression in unfractionated lung tissue, lung ECs, and ATII cells and alveolar macrophages (MØ). Lineage-specific markers were used to verify enrichment of isolated macrophages (*Emr1*, encoding F4/80 antigen), ECs (*Cdh5*), and ATII cells (*Sftpa*). Error bars represent SD.
See also Figures S1 and S2.

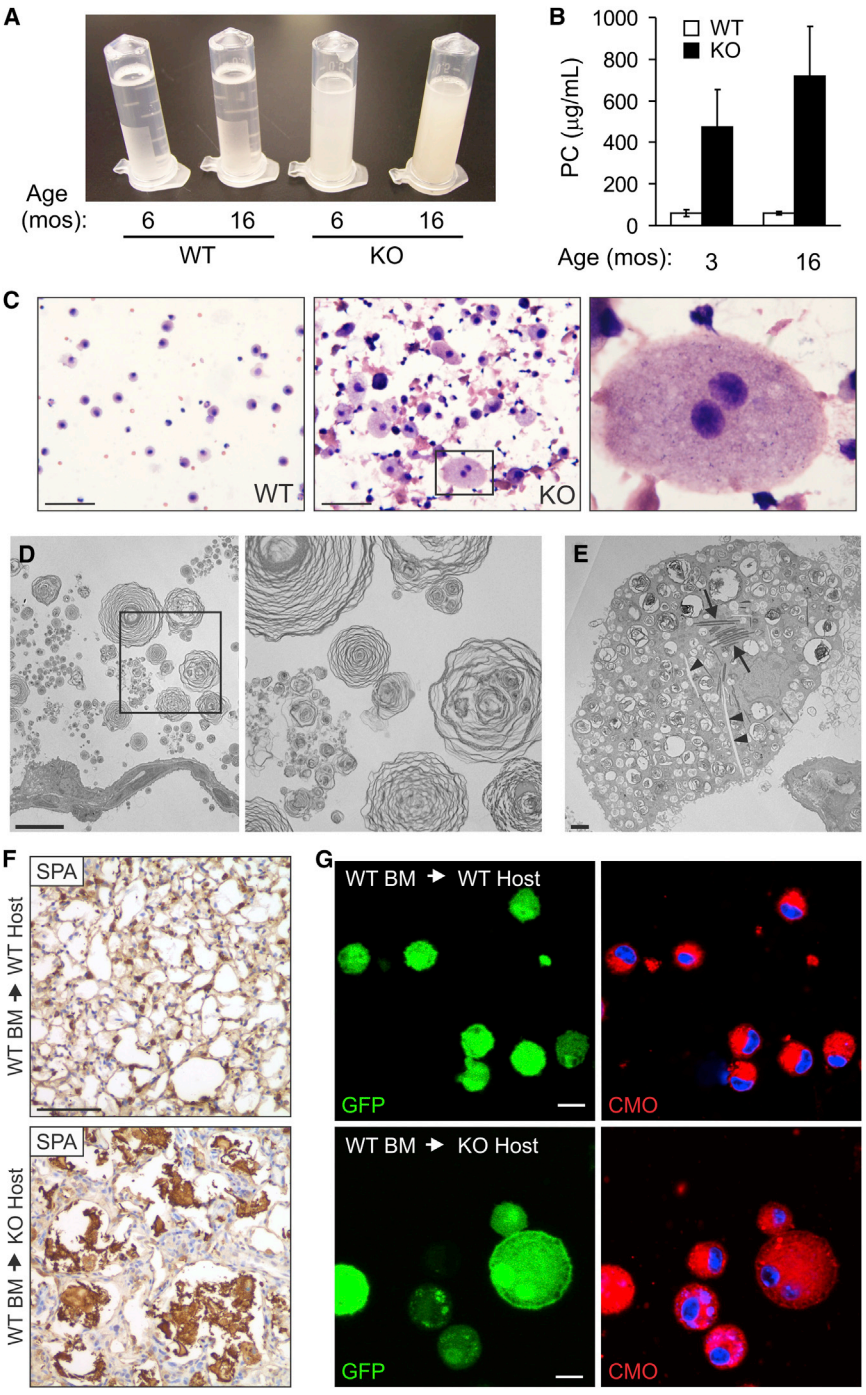

Figure 2. Foamy Macrophages Result from Changes in the Alveolar Microenvironment and Are Not Caused by GPR116 Loss in Macrophages

(A) Clarity of BALF was evaluated in *Gpr116* WT and KO mice.

(B) PC levels were quantified in KO versus WT BALF at 3 and 16 months ($p < 0.01$). Error bars represent SD.

(C) H&E of BALF from WT and KO mice. Approximately half of the macrophages in the KO were enlarged and foamy, and a smaller fraction (~3%) was binucleate (inset). Scale bar, 50 μm.

(D) Ultrastructural analysis of surfactant in the alveolar space of *Gpr116* KO lungs. Scale bar, 10 μm.

(E) Ultrastructural analysis of macrophages with surfactant-laden phagosomes. Macrophages contained rod-shaped electron-dense inclusions (arrows) similar to those in *Sftpa* transgenic mice (Elhalwagi et al., 1999), possibly Ym1 crystals, as well as electron-transparent cholesterol clefts (arrowheads). Scale bar, 2 μm.

(F) SP-A immunohistochemistry performed on lungs following BM transplantation. The transfer of *Gpr116* WT BM into KO mice failed to prevent the accumulation of SP-A+ material in the alveolar space. Scale bar, 100 μm

(G) Immunofluorescence performed on BALF following BM transplantation. An accumulation of enlarged, occasionally binucleate, macrophages was observed 6 months following the transfer of WT BM into the KO host. GFP expression of BALF cells confirms their origin from GFP-positive WT donor mice. To visualize all BM cells, membranes were labeled with CellMask Orange (CMO; red) and nuclei with DAPI (blue). Scale bar, 10 μm.

See also Figure S3.

Although the *SFTPC* promoter is predominantly expressed by ATII cells in adult mice, during embryogenesis, *SFTPC-Cre* is also expressed in early endoderm, leading to permanent Cre-mediated deletion of floxed genes in all respiratory epithelium including ATI cells (Okubo et al., 2005). To restrict the deletion to ATII cells, we further generated doxycycline-inducible *SFTPC*-driven *Gpr116* conditional KO mice that contained a floxed *Gpr116* allele and both the *tetO-Cre* and *SFTPC-rtTA* transgenes. Following doxycycline induction, we observed an accumulation of surfactant in the alveoli of *SFTPC* conditional *Gpr116* KO mice (*Gpr116*$^{-/flox}$; *Tg(SFTPC-rtTA/tetO-Cre)*), but not control mice that retained a WT *Gpr116* allele (*Gpr116*$^{-/+}$; *Tg(SFTPC-rtTA/tetO-Cre)*) (Figure 3B). Furthermore, in the BALF of the conditional KO, we detected an accumulation of SPA, SP-B, SP-C, and SP-D by western blotting and an elevation of PC and cholesterol by ELISA (Figures 3C and 3D), recapitulating each of the major phenotypes observed in the global KO. Taken together with the previous GPR116 expression analysis (Figures 1E–1G and S2D), we conclude that specific loss of GPR116 expression in ATII cells is responsible for the lung defects observed in global KO mice.

To explore the subcellular location of GPR116, we tagged GPR116 with GFP (GPR116-GFP) and expressed the fusion protein in A549 lung cells, a LB-containing cell line derived from ATII cells (Lieber et al., 1976). GPR116 was found to reside

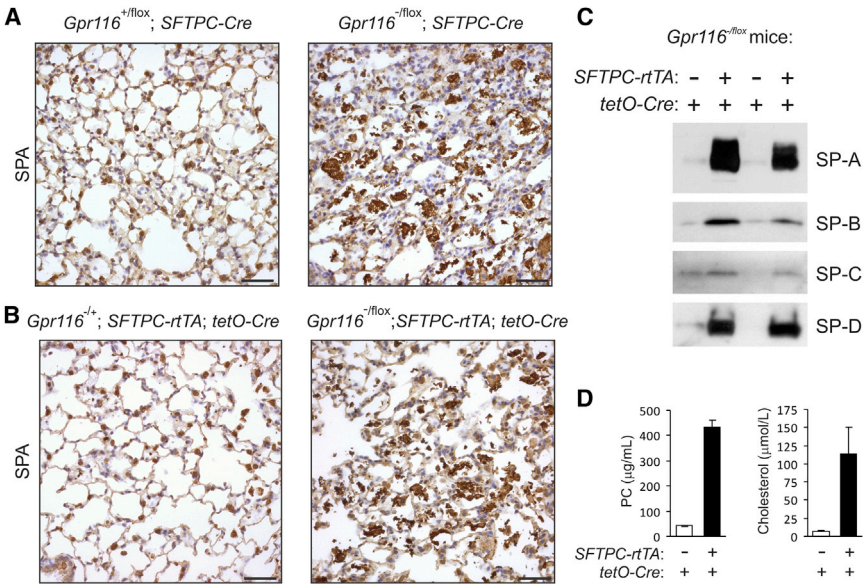

Figure 3. GPR116 Expression in ATII Cells Is Important for Lung Surfactant Homeostasis

(A) Surfactant accumulation in the alveolar space was assessed following constitutive *SFTPC-Cre*-mediated deletion. Scale bars, 50 μm.

(B) Surfactant accumulation in the alveolar space was assessed following doxycycline-inducible *SFTPC-Cre*-mediated deletion. Scale bars, 50 μm.

(C) Immunoblotting for SP-A, SP-B, SP-C, and SP-D in BALF derived from *Gpr116*$^{-/flox}$ conditional KO mice containing the indicated transgenes.

(D) PC and total cholesterol levels were quantified in WT versus KO BALF at 1 year of age (n = 3; $p < 0.01$). Error bars represent SD.

See also Figure S4.

predominantly in cytoplasmic vesicles with additional, limited expression at the cell surface (Figure 4A). This expression pattern was confirmed by both immunofluorescence (using GPR116 N-terminal Flag-tagged and C-terminal pyo-tagged vectors) and cell surface biotinylation studies (data not shown). Coimmunofluorescence labeling of GPR116 with ABCA3, a receptor that has been localized to the LB-limiting membrane (Mulugeta et al., 2002), revealed partial colocalization in LBs (Figure 4B). Thus, GPR116 resides both in LBs and at the cell surface, consistent with KO abnormalities both in the alveolar space (Figures 1B, 1C, and S2B) and inside the ATII cell (Figure S4).

GPR116 Is Required for Surfactant Uptake into ATII Cells

To understand the basis of the alveolar surfactant protein accumulation, we began by evaluating the mRNA levels of surfactant proteins in isolated ATII cells. We observed either no alteration in the KO (*Sftpb*, *Sftpc*, and *Sftpd*) or a 50% decrease (*Sftpa*) in expression (Figure 4C). Similarly, QPCR failed to detect any increase in expression of genes involved in lipid synthesis or transport in the KO lung, including *Abca3*, *Pcyt1a*, *Fasn*, *Gpam*, *Hmgcr*, and *Srebf2* (data not shown). We also failed to detect any increase in radiolabeled PC in the KO alveolar space following intravenous injection of ^{14}C-choline into *Gpr116* WT or KO mice (data not shown). Next, we examined SP-A and SP-B protein levels in isolated ATII cells and detected either no differences between WT and KO (SP-B) or a decrease in the KO (SP-A), in striking contrast to the clear increase observed in KO BALF and total lung lysates (Figure 4D). Furthermore, metabolic labeling of SP-A, the most overexpressed surfactant protein in the KO, revealed a slightly reduced production by *Gpr116* KO ATII cells (Figure 4E).

Although immunohistochemistry revealed predominant expression of SP-A in ATII cells of WT lung, in the KO, SP-A staining localized predominantly to the alveolar space and was barely detectable inside ATII cells (Figure 1B), suggesting that reuptake into ATII cells may be impaired. Because individual surfactant components were overexpressed to variable degrees in the KO lung (Figure 1D), we hypothesized that the altered surfactant composition could result in defective uptake. We obtained further evidence that surfactant composition was altered when we found that a polyclonal anti-SPA antibody that readily immunoprecipitated SP-A from *Gpr116* WT lung lavage only immunoprecipitated a small fraction of SP-A from the KO surfactant (Figure 4F). Importantly, SP-A immunoprecipitation from the KO was rescued following lipid extraction of the surfactant with butanol, revealing an abnormal association of SP-A with lipids that presumably resulted in epitope masking (Figure 4F). These results suggested that the phospholipid composition may be altered in the *Gpr116* KO. To investigate this possibility further, we isolated BALF from either 6-week-old or 6-month-old *Gpr116* WT or KO mice and performed lipidomics analysis using electrospray ionization mass spectrometry (ESI-MS) (Figures 4G–4J; Tables S1 and S2) (Ivanova et al., 2007; Myers et al., 2011). These studies revealed that the total amount of phospholipids in the BALF increased rapidly in *Gpr116* KO versus WT mice (5.9-fold by 6 weeks of age) and preceded the large increase in surfactant proteins that occurred by 6 months of age (Figures 4G–4J). An analysis of the different surfactant phospholipid classes, including PC, phosphatidylethanolamine (PE), phosphatidylglycerol (PG), phosphatidylinositol (PI), and phosphatidylserine (PS), revealed that the total levels of each were significantly increased in KO BALF, ranging from 4.1-fold (PS) to 9.7-fold (PI). Modest but significant changes in the ratio of PE, PI, and PS were also detected by 6 weeks of age (Figure 4I). Furthermore, an analysis of the individual lipid species within each class revealed an unexpected shift from saturated or monounsaturated fatty acids (FAs) to polyunsaturated FAs (Figure 4J; Table S1). A significantly increased amount of saturated lysophospholipids was also detected in the KO BALF (Table S2). Further studies are required to determine if reacylation of lysophospholipids is impaired or degradation of phospholipids by phospholipases is enhanced in the KO. Taken together, these studies reveal multiple and extensive changes in the phospholipid

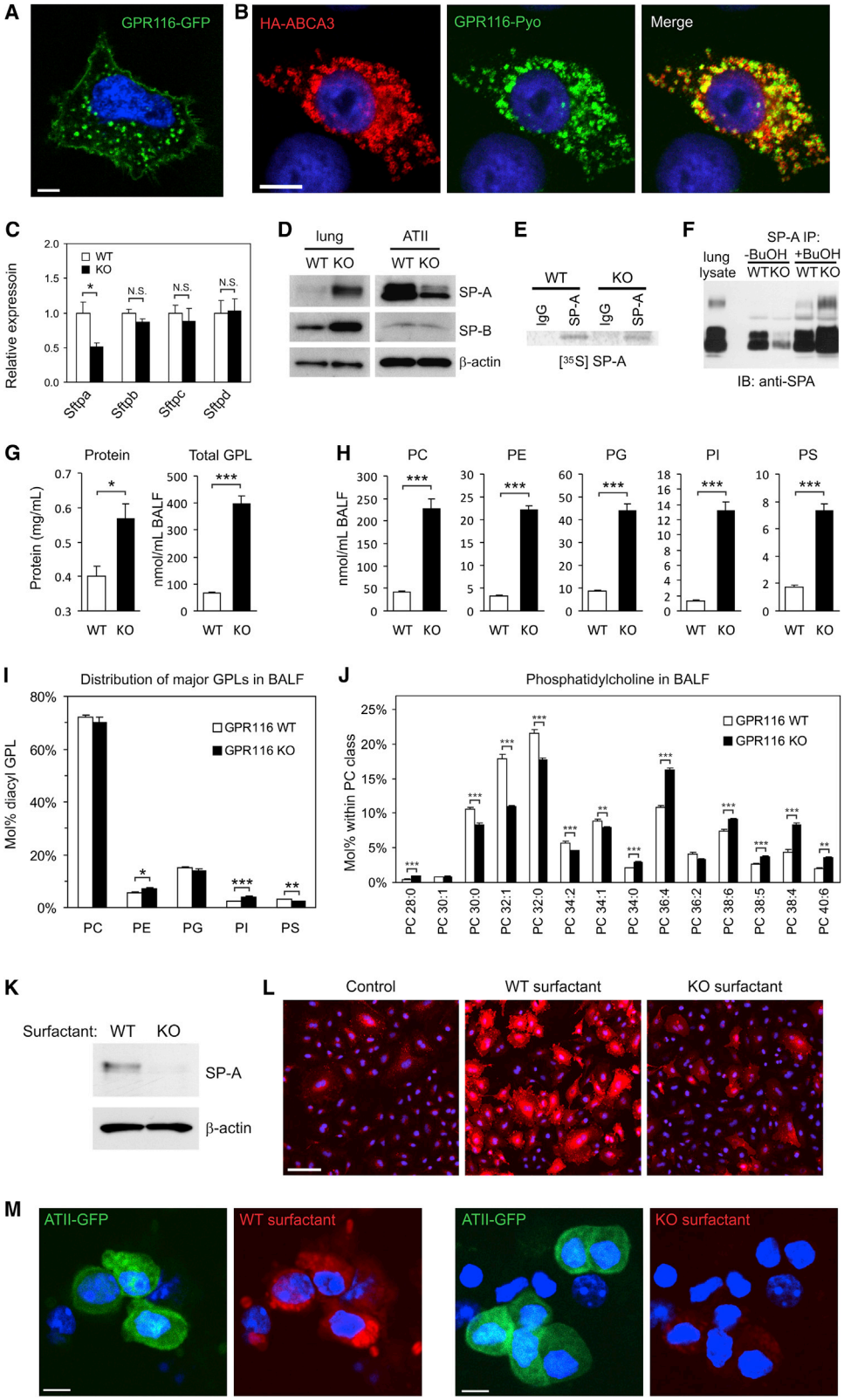

(legend on next page)

composition of *Gpr116* KO surfactant that potentially impact its biophysical properties.

Next, we sought to determine if the altered surfactant composition impacts uptake of surfactant proteins or lipids into ATII cells. First, we isolated equivalent amounts of WT or KO surfactant, spiked it with purified human SP-A, and then monitored SP-A uptake into freshly isolated ATII cells by immunoblotting using an anti-human SP-A mouse monoclonal antibody. The antibody employed does not cross-react with mouse SP-A, enabling us to track uptake of the exogenous human SP-A protein without interference from endogenous mouse SP-A. As shown if Figure 4K, these studies reveal that SP-A/WT surfactant was taken up by the ATII cells more efficiently than the SPA/KO surfactant. Next, we labeled the surfactant from WT or KO BALF with rhodamine and examined uptake into both A549 cells and GFP-positive ATII cells from SPC-GFP mice. In both models, WT surfactant was taken up more rapidly than KO surfactant (Figures 4L and 4M), although uptake into alveolar macrophages was unaffected. Taken together, these results indicate that GPR116 plays a role in regulating surfactant uptake by ATII cells, which is related, at least in part, to an abnormal surfactant assembly and composition.

Here, we provide evidence that GPR116 plays a highly specific, essential role in lung surfactant homeostasis and provide a mouse model for studying PAP driven by an autonomous ATII cell defect. The involvement of a GPCR family member in surfactant regulation has important implications for the understanding and treatment of lung surfactant disorders.

EXPERIMENTAL PROCEDURES

Animals

Mice were housed in a pathogen-free facility certified by the Association for Assessment and Accreditation of Laboratory Animal Care International, and the study was carried out in accordance with protocols approved by the NCI Animal Care and Use Committee. Further details on gene-targeting strategies and animal experiments are described in Extended Experimental Procedures.

Human Lung Tissues

The anonymized human lung tissue samples were obtained from the Cooperative Human Tissue Network with approval from the NIH Office of Human Subject Research. Nonmalignant lung tissues were derived from excess lung material removed at the time of surgical tumor removal. The histological staining methods are described in Extended Experimental Procedures.

Immunoblotting

Immunoblotting was performed as previously described by Nanda et al. (2004) using antibodies from Millipore against SP-A (AB3420), SP-B (AB3780), SP-C (AB3786), and SP-D (AB3434). Additional anti-SPA antibodies were purchased from Santa Cruz Biotechnology (sc-7699), Abcam (ab115791), and United States Biological (S8400-02).

Statistical Analysis

Unless stated otherwise, differences between two groups (for example, *Gpr116* WT and KO) were presented as the average ± SEM, and statistical significance was calculated using a Student's t test. For comparisons among multiple groups, a one-way ANOVA was used with a Bonferroni posttest. The p values <0.05 were considered significant.

SUPPLEMENTAL INFORMATION

Supplemental Information includes Extended Experimental Procedures, four figures, and three tables and can be found with this article online at http://dx.doi.org/10.1016/j.celrep.2013.04.019.

ACKNOWLEDGMENTS

This manuscript is dedicated to the memory of our dear friend and colleague Dr. Jo Rae Wright, who provided helpful advice and *SFTPC-GFP* mice for these studies. We thank Brigid L.M. Hogan and Jason R. Rock for providing *SFTPC-Cre* mice. This research was supported by the Center for Cancer Research Intramural Program, National Cancer Institute (NCI), National Institutes of Health, a part of the U.S. Department of Health and Human Services, and with federal funds from the NCI under contract nos. HHSN261200800001E and NIH HL34788. The content of this publication does not necessarily reflect the views or policies of the DHHS, nor does mention of trade names, commercial products, or organizations imply endorsement by the U.S. Government. Partial support for the lipidomic analysis was provided by an award from the NIGMS (U54 GM069338 to H.A.B.).

Figure 4. *Gpr116* Disruption Leads to a Defect in Surfactant Uptake by ATII Cells

(A) GPR116-GFP expression is localized to the cell surface and LB-like structures in A549 cells. Scale bar, 5 μm.

(B) Immunofluorescence staining was used to evaluate colocalization of GPR116 (green) with ABCA3 (red) in A549 cells. The merged image shows partial colocalization (yellow) in LB-like structures. In this experiment, cells were permeabilized to detect ABCA3, which resulted in reduced staining of GPR116 at the cell surface. Scale bar, 10 μm.

(C) QPCR analysis of purified ATII cells for SP-A, SP-B, SP-C, and SP-D at 6 weeks (n = 3).

(D) Immunoblotting of SP-A and SP-B in whole-lung lysates or isolated ATII cells derived from 6-week-old *Gpr116* KO versus WT mice. β-Actin was used as a loading control.

(E) Metabolic labeling of SP-A protein in ATII cells derived from *Gpr116* WT and KO lungs.

(F) Immunoprecipitation (IP) of SP-A with rabbit anti-SPA antibodies. Note the efficient IP of SP-A from *Gpr116* KO BALF required butanol (BuOH) extraction. IB, immunoblot.

(G) Total protein and total glycerophospholipid (GPL) levels were quantified in BALF from 6-week-old WT or KO mice (n = 5).

(H) Total PC, PE, PG, PI, and PS levels were quantified in BALF from 6-week-old WT or KO mice (n = 5).

(I) The relative distribution of GPLs was quantified in BALF from 6-week-old WT or KO mice (n = 5). %Mol, molar percentage.

(J) The individual PC species were quantified in BALF from 6-week-old WT or KO mice (n = 5). The PC species are labeled according to the total number of carbons in their FA chains followed by the number of double bonds in the FA chains.

(K) Purified human SP-A was mixed with surfactant from WT or KO mice, and uptake into isolated ATII cells was monitored by immunoblotting with mouse anti-human SP-A antibodies. β-Actin was used as a loading control.

(L) Uptake of rhodamine-PE-labeled WT or KO surfactant was evaluated in A549 cells. The control represents rhodamine-PE alone. Scale bar, 100 μm.

(M) Uptake of rhodamine-PE-labeled WT or KO surfactant was evaluated in ATII-enriched cell fractions from SPC-GFP transgenic mice. In this particular experiment, GFP-positive ATII cells (green) were not sorted by flow cytometry, but a partial enrichment of ATII cells was achieved by magnetic depletion of hematopoietic cells and ECs. Scale bars, 5 μm.

Error bars represent SD (C) or SEM (G–J). *$p < 0.05$, **$p < 0.01$, ***$p < 0.001$.

See also Tables S1 and S2.

Cell PRESS
Open ACCESS

Received: August 21, 2012
Revised: April 8, 2013
Accepted: April 19, 2013
Published: May 16, 2013

REFERENCES

Abe, J., Suzuki, H., Notoya, M., Yamamoto, T., and Hirose, S. (1999). Ig-hepta, a novel member of the G protein-coupled hepta-helical receptor (GPCR) family that has immunoglobulin-like repeats in a long N-terminal extracellular domain and defines a new subfamily of GPCRs. J. Biol. Chem. *274*, 19957–19964.

Borie, R., Danel, C., Debray, M.P., Taille, C., Dombret, M.C., Aubier, M., Epaud, R., and Crestani, B. (2011). Pulmonary alveolar proteinosis. Eur. Respir. Rev. *20*, 98–107.

Carey, B., and Trapnell, B.C. (2010). The molecular basis of pulmonary alveolar proteinosis. Clin. Immunol. *135*, 223–235.

Elhalwagi, B.M., Zhang, M., Ikegami, M., Iwamoto, H.S., Morris, R.E., Miller, M.L., Dienger, K., and McCormack, F.X. (1999). Normal surfactant pool sizes and inhibition-resistant surfactant from mice that overexpress surfactant protein A. Am. J. Respir. Cell Mol. Biol. *21*, 380–387.

Ivanova, P.T., Milne, S.B., Byrne, M.O., Xiang, Y., and Brown, H.A. (2007). Glycerophospholipid identification and quantitation by electrospray ionization mass spectrometry. Methods Enzymol. *432*, 21–57.

Lewis, J.F., and Veldhuizen, R.A. (2006). The future of surfactant therapy during ALI/ARDS. Semin. Respir. Crit. Care Med. *27*, 377–388.

Lieber, M., Smith, B., Szakal, A., Nelson-Rees, W., and Todaro, G. (1976). A continuous tumor-cell line from a human lung carcinoma with properties of type II alveolar epithelial cells. Int. J. Cancer *17*, 62–70.

Malur, A., Baker, A.D., McCoy, A.J., Wells, G., Barna, B.P., Kavuru, M.S., Malur, A.G., and Thomassen, M.J. (2011a). Restoration of PPARγ reverses lipid accumulation in alveolar macrophages of GM-CSF knockout mice. Am. J. Physiol. Lung Cell. Mol. Physiol. *300*, L73–L80.

Malur, A., Huizar, I., Wells, G., Barna, B.P., Malur, A.G., and Thomassen, M.J. (2011b). Lentivirus-ABCG1 instillation reduces lipid accumulation and improves lung compliance in GM-CSF knock-out mice. Biochem. Biophys. Res. Commun. *415*, 288–293.

Mulugeta, S., Gray, J.M., Notarfrancesco, K.L., Gonzales, L.W., Koval, M., Feinstein, S.I., Ballard, P.L., Fisher, A.B., and Shuman, H. (2002). Identification of LBM180, a lamellar body limiting membrane protein of alveolar type II cells, as the ABC transporter protein ABCA3. J. Biol. Chem. *277*, 22147–22155.

Myers, D.S., Ivanova, P.T., Milne, S.B., and Brown, H.A. (2011). Quantitative analysis of glycerophospholipids by LC-MS: acquisition, data handling, and interpretation. Biochim. Biophys. Acta *1811*, 748–757.

Nanda, A., Carson-Walter, E.B., Seaman, S., Barber, T.D., Stampfl, J., Singh, S., Vogelstein, B., Kinzler, K.W., and St Croix, B. (2004). TEM8 interacts with the cleaved C5 domain of collagen alpha 3(VI). Cancer Res. *64*, 817–820.

Okubo, T., Knoepfler, P.S., Eisenman, R.N., and Hogan, B.L. (2005). Nmyc plays an essential role during lung development as a dosage-sensitive regulator of progenitor cell proliferation and differentiation. Development *132*, 1363–1374.

Raghavendran, K., Willson, D., and Notter, R.H. (2011). Surfactant therapy for acute lung injury and acute respiratory distress syndrome. Crit. Care Clin. *27*, 525–559.

Sakagami, T., Uchida, K., Suzuki, T., Carey, B.C., Wood, R.E., Wert, S.E., Whitsett, J.A., Trapnell, B.C., and Luisetti, M. (2009). Human GM-CSF autoantibodies and reproduction of pulmonary alveolar proteinosis. N. Engl. J. Med. *361*, 2679–2681.

Seaman, S., Stevens, J., Yang, M.Y., Logsdon, D., Graff-Cherry, C., and St Croix, B. (2007). Genes that distinguish physiological and pathological angiogenesis. Cancer Cell *11*, 539–554.

Shibata, Y., Berclaz, P.Y., Chroneos, Z.C., Yoshida, M., Whitsett, J.A., and Trapnell, B.C. (2001). GM-CSF regulates alveolar macrophage differentiation and innate immunity in the lung through PU.1. Immunity *15*, 557–567.

St Croix, B., Rago, C., Velculescu, V., Traverso, G., Romans, K.E., Montgomery, E., Lal, A., Riggins, G.J., Lengauer, C., Vogelstein, B., and Kinzler, K.W. (2000). Genes expressed in human tumor endothelium. Science *289*, 1197–1202.

Tang, X.L., Wang, Y., Li, D.L., Luo, J., and Liu, M.Y. (2012). Orphan G protein-coupled receptors (GPCRs): biological functions and potential drug targets. Acta Pharmacol. Sin. *33*, 363–371.

Trapnell, B.C., Whitsett, J.A., and Nakata, K. (2003). Pulmonary alveolar proteinosis. N. Engl. J. Med. *349*, 2527–2539.

Wallgard, E., Larsson, E., He, L., Hellström, M., Armulik, A., Nisancioglu, M.H., Genove, G., Lindahl, P., and Betsholtz, C. (2008). Identification of a core set of 58 gene transcripts with broad and specific expression in the microvasculature. Arterioscler. Thromb. Vasc. Biol. *28*, 1469–1476.